A review of Residual distribution schemes for hyperbolic and parabolic problems: the july 2010 state of the art

Rémi Abgrall

INSTITUT NATIONAL DE RECHERCHE EN INFORMATIQUE ET EN AUTOMATIQUE

A review of Residual distribution schemes for hyperbolic and parabolic problems : the july 2010 state of the art

Rémi Abgrall

N° 7419

July 2010

Thème NUM

ISSN 0249-6399 ISRN INRIA/RR--7419--FR+ENG

INSTITUT NATIONAL
DE RECHERCHE
EN INFORMATIQUE
ET EN AUTOMATIQUE

INRIA

centre de recherche
BORDEAUX - SUD OUEST

A review of Residual distribution schemes for hyperbolic and parabolic problems : the july 2010 state of the art

Rémi Abgrall

Thème NUM — Systèmes numériques
Équipes-Projets BACCHUS

Rapport de recherche n° 7419 — July 2010 — 36 pages

Abstract: We describe and review (non oscillatory) residual distribution schemes that are rather natural extension of high order finite volume schemes when a special emphasis is put on the structure of the computational stencil. We provide their connections with standard stabilized finite element and discontinuous Galerkin schemes, show that their are really non oscillatory. We also discuss the extension to these methods to parabolic problems. We also draw some research perspectives.

Key-words: Residual distribution methods, non oscillatory schemes, hyperbolique and parabolic problems, unstructured meshes.

Centre de recherche INRIA Bordeaux – Sud Ouest
Domaine Universitaire - 351, cours de la Libération 33405 Talence Cedex
Téléphone : +33 5 40 00 69 00

État de l'art, en juillet 2010, sur les schémas distribuant le résidu pour les problèmes hyperboliques et paraboliques.

Résumé : We describe and review (non oscillatory) residual distribution schemes that are rather natural extension of high order finite volume schemes when a special emphasis is put on the structure of the computational stencil. We provide their connections with standard stabilized finite element and discontinuous Galerkin schemes, show that their are really non oscillatory. We also discuss the extension to these methods to parabolic problems. We also draw some research perspectives.

Mots-clés : Schémas distribuant le résidus, schémas non oscillants, problèmes hyperboliques et paraboliques, maillages non structurés.

Contents

1 Introduction.

The numerical simulation of compressible flow problems, or more generally speaking, of partial differential equations (PDEs) of hyperbolic nature, has been the topic of a huge literature since the seminal work of von Neuman in the 40's. Among the "hot" topics of the field has been, since the works of Lax, Wendroff, Godunov, Mc Cormack, van Leer, Roe, A. Harten, Yee and Osher, to give a few names, the development of robust, parameter free and accurate schemes. Among the most successful methods one may quote the van Leer's MUSCL method [32] and modified flux approach of Roe. These techniques are only second order accurate. The accuracy can be improved via the ENO/WENO methods by Harten, Shu and others.

The emergence of modern parallels computers, another concern has emerged: what about accuracy and efficiency ? Indeed, it is now important to develop robust algorithms that scales correctly on parallel architecture. This can be achieved more or less easily if the stencil of the numerical scheme is as compact as possible. Good candidates are the schemes relying on finite element technology, such as the Discontinuous Galerkin (DG) methods [11] or the stabilized continuous finite element(CFE) methods [20, 19]. In these methods, the numerical stencil is the most possible compact one.

In these notes, we discuss in some details of another class of numerical schemes, the so-called Residual Distribution schemes (RD for short), also denoted by Fluctuation Splitting schemes. The history of these schemes can be traced back to the work of P.L. Roe [28] and even his famous 1981 paper [29] where he does not define a finite volume scheme but a true residual distribution scheme. Indeed, the first RD scheme ever was probably presented by Ni [22]. The idea was to construct a scheme with the most compact computational stencil that can ensure second order accuracy. This scheme had some similarities with the Lax Wendroff one.

If these RD share many similarities with more established schemes such as the SUPG scheme by Hughes and coworkers [17, 18, 19], the driving idea is (i) to introduce the upwinding concept, (ii) to manage such that a provable or a practical maximum principle is achieved without any parameter to tune. In our opinion, (ii) is the most important feature.

In Roe's paper and the first RD papers, the main idea was to introduce upwinding into the numerical formulation of the problems, coupled in a very clever way, with a technique to reach second order accuracy for steady problem. This has been presented in a serie of papers and VKI reports, see e.g. [12, 13, 30, 14, 31, 23]. Two schemes had emerged at the time : the N scheme by Roe and the PSI scheme by R. Struijs, see [14]. The first one is probably the optimal first order strategy for scalar problems using triangular meshes, the second one the best second order scheme on these type of meshes, for steady problems again. When dealing with systems or non triangular meshes, the situation became more complex, and it appears that the upwinding concept has to be relaxed a bit.

This paper presents a personal view of what is the current status of RD scheme for *steady* problems. In a first part, I present a reinterpretation of standard finite volume schemes. Then I give a very formal variational formulation and some connection with more established schemes such as the Discontinuous Galerkin schemes or the stabilised continuous finite element. In a second part, I discuss a systematic way of getting a non oscillatory scheme, without tunable parameter, even in the system case. Numerical examples are given for illustration. The last section is devoted to some extensions, in particular the unsteady case and the viscous case.

2 About finite volume schemes and their connections to RD schemes.

2.1 Re-formulation of finite volume schemes.

Let us start with a simple example. We consider the following problem

$$\frac{\partial u}{\partial t} + \frac{\partial f(u)}{\partial x} = 0 \tag{1}$$

with initial and boundary conditions that we do not specify for the moment. Using a regular mesh ($x_j = j\Delta x$), this problem is discretised by a simple finite volume scheme

$$\Delta x \, \frac{u_i^{n+1} - u_i^n}{\Delta t} + F_{i+1/2} - F_{i-1/2} = 0 \tag{2}$$

where $F_{j+1/2}$ is the numerical flux at the cell interface $x_{j+1/2} = \frac{x_j + x_{j+1}}{2}$. It depends on the local cell averages of the solution $\{u_l\}_{l=j-p}^{j+p}$, where

$$u_j \approx \frac{\int_{x_{j-1/2}}^{x_{j+1/2}} u(x,t)dx}{\Delta x}.$$

We can rewrite (2) as

$$\Delta x \, \frac{u_i^{n+1} - u_i^n}{\Delta t} + \phi_{i+1/2}^- + \phi_{i-1/2}^+ = 0 \tag{3}$$

where we have set

$$\phi_{i+1/2}^- = F_{i+1/2} - f(u_i), \qquad \phi_{i-1/2}^+ = f(u_i) - F_{i-1/2}.$$

In each interval $[x_i, x_{i+1}]$, we have introduced the "residuals"

$$\phi_{i+1/2}^- = F_{i+1/2} - f(u_i), \qquad \phi_{i+1/2}^+ = f(u_{i+1}) - F_{i+1/2}. \tag{4}$$

The two formulations (2) and (3) are of course equivalent.

If the numerical scheme $F_{j+1/2}$ is consistent with the continuous one, and depends continuously of its arguments, assuming in addition some stability assumptions, the Lax Wendroff theorem states that the solution of (2) converges to a weak solution of (1). In the proof of this theorem, the key algebraic argument is that $F_{i+1/2} - F_{i-1/2}$ is a difference of flux. Considering now (4), this argument is translated into the relation

$$\phi_{i+1/2}^- + \phi_{i+1/2}^+ = f(u_{i+1}) - f(u_i) = \int_{x_i}^{x_{i+1}} \frac{\partial f(u^{\Delta x})}{\partial x} dx \tag{5}$$

where $u^{\Delta x} = u_i \frac{x_{i+1} - x}{\Delta x} + u_{i+1} \frac{x_i - x}{\Delta x}$. On can show, see for example [6] for a more complex case, that under the assumptions of the Lax Wendroff theorem (stability assumptions, and continuous dependency of the residuals with respect to their arguments), that the solution of (3) converges to a weak solution of (1).

2.2 About accuracy.

The goal is to construct schemes of the type (3)-(5) that have the most possible compact stencil with the maximum accuracy. We show here that there is some hope. For example, second order accuracy can be obtained with a 3 point stencil (instead of 5 for a standard high order scheme). This is done in two steps. We first consider the steady version of (1) and then extend the method to the unsteady case. Of course the steady version of (1) is trivial, but is rather enlighting to consider the following problem

$$\begin{aligned} u' &= \lambda u \qquad x \in]0,1] \\ u(0) &= 1. \end{aligned} \tag{6}$$

The solution of (6) is $u(x) = e^{\lambda x}$.

If one wishes to approximate (6) by an upwind finite volume, a natural formulation is

$$F_{i+1/2} - F_{i-1/2} = \lambda \int_{x_{i-1/2}}^{x_{i+1/2}} u(x)dx \approx \Delta x \lambda u_i.$$

Note that the source term is approximated with second order accuracy, and $F_{i+1/2} = u_i$, $F_{i-1/2} = u_{i-1}$. The scheme is

$$u_i - u_{i-1} = \Delta x \lambda u_i, \qquad u_0 = 1. \tag{7}$$

We obtain $u_i = \left(1 - \lambda \frac{x_i}{i}\right)^i$: if i is chosen so that $x_i = i\Delta x$ is *fixed*, $u_i - u(x_i) = \frac{1}{2} e^{\lambda x_i} x_i \lambda^2 \Delta x + O(\Delta x^2)$: the convergence is only first order.

Consider now the scheme

$$u_i - u_{i-1} - \frac{\lambda \Delta x}{2}(u_i + u_{i-1}) = 0 \qquad \text{with } u_0 = 1. \tag{8}$$

We get

$$u_i = \left(\frac{1 + \frac{\lambda \Delta x}{2}}{1 - \frac{\lambda \Delta x}{2}}\right)^i$$

so that when i is chosen with $x_i = i\Delta x$ *fixed*,

$$u_i - u(x_i) = \frac{1}{12} e^{\lambda x_i} \lambda^3 x_i \Delta x^2 + O(\Delta x^4)$$

which shows so the convergence is second order. The scheme (8) can be interpreted in the residual distribution framework. To do that, we define the total residual by

$$\phi_{i+1/2} = \int_{x_i}^{x_{i+1}} \left((u^{\Delta x})' - \lambda u^{\Delta x}\right) dx = u_{i+1} - u_i - \lambda \frac{u_i + u_{i+1}}{2}$$

and the sub-residuals by

$$\phi^-_{i+1/2} = \phi_{i+1/2}, \qquad \phi^+_{i+1/2} = 0$$

i.e., we distribute on the downwind vertex of the cell $[x_i, x_{i+1}]$.

This simple example shows that one can maximize accuracy with the smallest stencil. This is precisely the philosophy that is pursued by the Residual Distribution schemes (RD schemes for short), with the goal of deriving non oscillatory schemes.

3 Relationships between Discontinuous Galerkin, stabilised Continuous Galerkin and RD schemes.

We show that another interpretation of (3) is a variational one and then generalise it in the multi dimensional case.

3.1 A variational formulation of the finite volume schemes.

We start again from (1) in the steady case, even though the solutions are trivial. Again, we neglect the boundary conditions for the sake of simplicity, and we assume the solution to be scalar.

Formaly, we introduce

$$\beta^-_{i+1/2} = \frac{F_{i+1/2} - f(u_i)}{f(u_{i+1}) - f(u_i)} \text{ and } \beta^+_{i+1/2} = \frac{f(u_{i+1}) - F_{i+1/2}}{f(u_{i+1}) - f(u_i)},$$

so that (3) becomes (in the steady case)

$$\beta^-_{i+1/2}(f(u_{i+1}) - f(u_i)) + \beta^+_{i-1/2}(f(u_{i+1}) - f(u_i)) = 0$$

If φ discontinuous and linear in each interval $[x_j, x_{j+1}]$[1], we have

$$\sum_j \{\beta^-_{j+1/2}\varphi_j + \beta^+_{j+1/2}\varphi_{j+1}\}(f(u_{j+1}) - f(u_j)) = 0. \tag{9}$$

We introduce the mapping $\pi^{\Delta x}$ from $V^{\Delta x}$ to $\widetilde{V}^{\Delta x}$ the set of functions that are constant on each interval $[x_j, x_{j+1}]$ but possibly discontinuous accross the cell interfaces. The function $\pi^{\Delta x}(\varphi)$ is, on $[x_j, x_{j+1}]$,

$$\pi^{\Delta x}(\varphi) = \beta^-_{j+1/2}\varphi_i + \beta^+_{j+1/2}\varphi_{j+1}.$$

The relation (9) can be reinterpreted, since $\pi^{\Delta x}$ is constant on $[x_j, x_{j+1}]$, as

$$\sum_j \left(\int_{\partial[x_j, x_{j+1}]} \pi^{\Delta x}(\varphi) f(u^{\Delta x}) dx - \int_{[x_j, x_{j+1}]} (\pi_{\Delta x}(\varphi))' f(u^{\Delta x}) dx \right) = 0. \tag{10}$$

The next natural question is to understand how can be constructed a set of coefficients $\beta^{\pm}_{j+1/2}$ such that the scheme defined by (10) is stable, non oscillatory and accurate. The one dimensional case, for second order accuracy, is very specific. Indeed, using the techniques presented in section 4 and more specifically when we wish to enforce automaticaly an non oscillatory behavior, we can show that in general $\beta^-_{j+1/2} = 0$ and $\beta^+_{j+1/2} = 1$: in a way, upwinding is built-in.

3.2 Generalisation to the multi dimensional case.

Inspired by the variational formulation (10), we can generalise it and show connections the method to more standard methods like the stream-line diffusion method or the Discontinuous Galerkin methods by playing with the couple test function/approximation space. We are given a triangulation $\mathcal{T}^h$, we assume that it is conformal, and denote by K a generic element of $\mathcal{T}^h$.

[1] $V^{\Delta x}$ is the set of these functions.

The "unfiltered" RD scheme are a direct extension of (10). It writes: find u^h continuous and polynomial of degree k (this space is called V^h) in each element of $\mathcal{T}^h$ such that for any $v^h \in V^h$

$$\sum_{\sigma\in\Omega} v^h(\sigma)\Big(\sum_{K\ni\sigma}\beta_\sigma^K\int_{\partial K} f(u^h)\cdot\vec{n}dl\Big)=0$$

Using conservation and after rearangement, we get

$$\sum_K \overbrace{\Big(\sum_{\sigma\in K}\beta_\sigma^K v_\sigma\Big)}^{\pi^h(v_h)}\int_{\partial K} f(u^h)\cdot\vec{n}dl=0$$

where

$$\begin{aligned}&\pi^h : V^h\to\widetilde{V}^h\\ &\quad v^h\mapsto\pi^h(v^h) \text{ such that on any element } K, \pi^h(v^h)_{|K}=\sum_{\sigma\in K}\beta_\sigma^K v_\sigma^h\end{aligned}$$

with $\widetilde{V}^h := \{w\in L^2,$ for any element $K, w_{|K}$constant $\}$. We note that $\pi(v^h)$ depends on v^h and u^h in general.

This algebra indicates that the "unfiltered" RD scheme can be seen as (because $\pi^h(v^h)$ is constant over any K)

$$\sum_K\Big(\int_{\partial K}\pi^h(v^h)f(u^h)\cdot\vec{n}dl-\overbrace{\int_K\nabla\pi^h(v^h)\cdot f(u^h)dx}^{=0}\Big)=0 \qquad (11)$$

The question is how to build the operator π^h (i.e. the coefficients $\{\beta_\sigma^K\}_{\sigma,K}$) such that the scheme is stable, consistant, converge to the correct weak solutions and has the most possible compact stencil. We examine this question in section (4).

However, in most cases, we can see experimentaly that the behavior of (11) is not as good as expected: spurious modes exist, and we need to remove them. The most efficient way to do so is to add a dissipative term that keep the accuracy. One particular example of such scheme is what we call the filtered RD scheme.

It writes: find $u^h\in V^h$ such that for any $v^h\in V^h$,

$$\begin{aligned}\sum_K\Big(\int_{\partial K}\pi^h(v^h)f(u^h)\cdot\vec{n}dl-\int_K\nabla\pi^h(v^h)\cdot f(u^h)dx\\ +h_K\int_K\big[\nabla_u f(u^h).\nabla v^h\big]\cdot\big[\nabla_u f(u^h).\nabla u^h\big]dx\Big)=0.\end{aligned} \qquad (12)$$

We easily see some connections with more standard methods.

The DG method (without limiter) is: find u^h, v^h in broken polynomial spaces

$$\sum_K\Big(\int_{\partial K} v^h\hat{f}(u^h)\cdot\vec{n}dl-\int_K\nabla v^h\cdot f(u^h)dxd\Big)=0$$

with $\hat{f}$ the numerical flux, while the stabilised FE methods (like SUPG) are find u^h, v^h in V^h such that

$$\sum_K \left(\int_{\partial K} v^h f(u^h) \cdot \vec{n} dl - \int_K \nabla v^h \cdot f(u^h) dx + h_K \int_K \left[\nabla_u f(u^h).\nabla v^h\right] \cdot \left[\nabla_u f(u^h).\nabla u^h\right] \right) = 0$$

So depending on which trial space and test functions, one can recover any method. The problem here is that the RD scheme generally uses test functions that depends on the solution. This abstract formulation is never used in the way these schemes are implemented in practice.

The next section is devoted to show how one can construct (11) such that the method is non oscillatory and conservative, then we show numerical examples for (11) and (12).

4 Residual distribution schemes.

4.1 Case of scalar problems.

4.1.1 The model problem.

We first consider the steady problem

$$\text{div } f(u) = 0 \text{ in } \Omega \subset \mathbb{R}^d \tag{13a}$$

subjected to Dirichlet boundary conditions on the inflow part Γ^- of $\Gamma = \partial\Omega$,

$$u = g \text{ in } \Gamma^- \tag{13b}$$

If $M \in \Gamma$ and $\vec{n}$ is the outward unit vector at M of Γ, the inflow boundary is defined as

$$\Gamma^- = \{M \in \Gamma, \nabla_u f(u(M)) \cdot \vec{n} < 0\}$$

4.1.2 Approximation space.

The domain Ω is triangulated by a conformal mesh, the triangulation is denoted by $\mathcal{T}_h$. The elements of this triangulation are triangles and quads in 2D, or tetrahedrons in 3D. Other types of elements could certainly be tackled, but this has not yet been done. The elements of $\mathcal{T}_h$ are denoted by $\{K_i\}_{i=1,n_e}$ and the vertices are denoted by $\{M_i\}_{i=1,n_s}$. In most cases, we deal with one generic element K; since there is no ambiguity, the vertices are denoted by $i = 1, n_K$ where n_k is the number of vertices in K.

The approximate solution of (13) will be sought for in the space

$$V^h = \{u \text{ continuous in } \Omega_h, \text{ for any } u_{|K} \text{ is polynomial of degree r.}\}.$$

In d dimensions, a polynomial of degree r is defined by $n_r^d = C_{d+r}^d$ coefficients, i.e. $\frac{(r+1)(r+2)}{2}$ in 2D and $\frac{(r+1)(r+2)(r+3)}{6}$ in 3D. This means that a polynomial is uniquely defined if an unisolvant set of points of cardinal n_r^d is given. In the case of triangles/tetrahedrons, the standard Lagrange points , for example by their barycentric coordinates $(\frac{i}{r}, \frac{j}{r}, \frac{k}{r})_{i,j,r \geq 0, i+j+r=d}$ in the case of a triangle and $(\frac{i}{r}, \frac{j}{r})_{i,j \geq 0, i+j \leq r}$ for a quad when it is mapped onto $[0,1]^2$. The Lagrange points are the degrees of freedom at which an approximation of u is sought for.

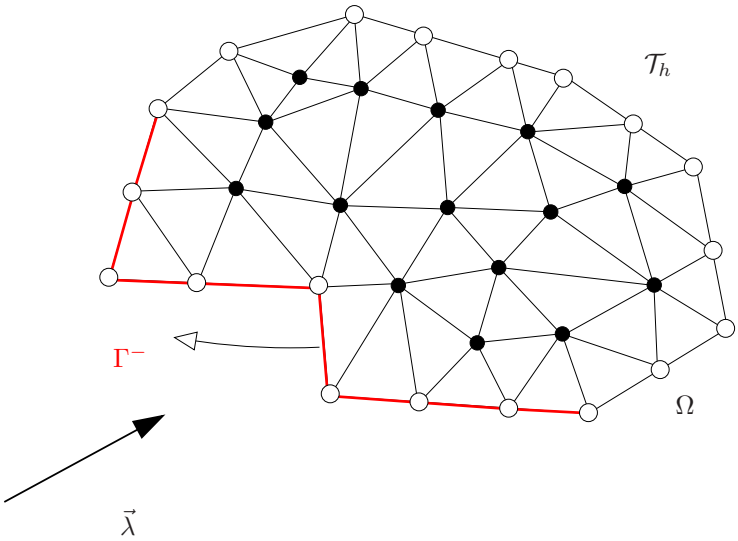

Figure 1: A typical mesh

The class of triangulations that we consider are regular in the finite element meaning, i.e. there is a constant $C_{\mathcal{T}}$ such that if ρ_K is the ratio of the outer diameter of K to the inner diameter of K (so $\rho_K \geq 1$),

$$\max_{K\in\mathcal{T}_h} \rho_K \leq C_{\mathcal{T}}. \tag{14}$$

As classical, the parameter "h" in $\mathcal{T}_h$ refers to the maximum of the diameters of the elements contained in $\mathcal{T}_h$.

4.1.3 Numerical discretisation.

The approximation is done in two steps. For any element K, we define the total residual

$$\phi_K(u^h) := \int_{\partial K} f(u^h)\cdot\vec{n}d\sigma \tag{15a}$$

which is splitted into the sub-residuals ϕ_j^K, one for each degree of freedom σ_j in K. Since there is no ambiguity, we denote these degrees of freedom by $j, j = 1,\ldots,n_K$. The sub-residuals are contrainted by the *conservation* relation

$$\sum_{\sigma_j\in K} \phi^K_{\sigma_j}(u^h) = \phi^K(u^h) \tag{15b}$$

The scheme writes : find $u^h \in V^h$ such that for any degree of freedom $\sigma \ni \Gamma^-$,

$$\sum_{K,\sigma\in K} \phi^K_{\sigma}(u^h) = 0 \tag{15c}$$

while on the boundary Γ^- we set

$$u^h(\sigma) = g(\sigma). \tag{15d}$$

Of course the problem (15) is in general a (very) non linear problem, which is in practice solved by an iterative technique. We later rapidly come back to this point.

There are a couple of general results which explain the type of structure the residuals and sub-residuals should have in order to guaranty accuracy and convergence to a weak solution of (13), if the method converges.

4.1.4 Convergence to a weak solution.

We have the following result that has been shown in [6].

Proposition 4.1. *We consider a family of triangulations that satisfy* (14) *such that* $h \to 0$. *Assume that the sub-residuals depend continuously on* u^h, *that there exists a constant* C *independent of* h *such that*

$$\max_{\sigma \in \mathcal{T}_h} |u^h(\sigma)| \leq C$$

and a function $v \in L^2(\Omega)$ *such that a sub sequence* $u^{h_{n_k}} \to v$ *in* $L^2(\Omega)$ *when* $k \to +\infty$. *Then* v *is a weak solution of* (13)

The key argument is the conservation relation (15b). In (15a), the integral is generally obtained by numerical quadrature and the result is independent of the numerical quadrature, provided that on any edge/face of $\mathcal{T}_h$, the set of quadrature points only depend on the edge/face and not on the particular element this edge/face is part of.

4.1.5 Accuracy constraints.

On an unstructured mesh, it is difficult, if not hopeless, to derive an error analysis via Taylor expansions, because the mesh has in general non geometrical symmetries. Hence, it is better to rely on a weak form of the truncation error. Consider φ a C^1 function on Ω with $||\varphi||_\infty \leq 1$. This inequality is set up for scaling purpose only. We define the truncation error for w^h, the interpolate of the exact solution of (13) (assuming it is smooth en ought) by

$$\mathcal{E}_h(u) = \max_{\varphi \in C^1(\Omega), ||\varphi||_\infty \leq 1, ||\nabla \varphi||_\infty \leq 1} \left(\sum_{\sigma \in \mathcal{T}_h} \varphi(\sigma) \Big(\sum_{K, \sigma \in K} \phi_\sigma^K \Big) \right) \tag{16a}$$

and the scheme is p-th order accurate if there exists a constant C independent of h such that

$$\mathcal{E}_h(u) \leq C h^p. \tag{16b}$$

There is a simple construction that permits, formally at least, to fulfill (16b), it relies on the use of the structure of (13) : it is a steady problem. The case of time dependent problem will be considered later. The key remark is that if for any σ and K, the sub-residuals (evaluated for an interpolation w^h of the exact solution, assuming it is smooth enough) satisfies

$$|\phi_\sigma^K(w^h)| \leq C h^{p+d} \tag{17}$$

where C is independent of $\mathcal{T}_h$ satisfying (14), then (16b) holds. Again the proof is given in [6], and we recall it shortly. We introduce the Galerkin residuals,

$$\phi_\sigma^{T,c} = \int_K \psi_\sigma \text{ div } f(u^h) dx$$

and we have

$$\sum_{\sigma\in\mathcal{T}_h}\varphi(\sigma)\Big(\sum_{K,\sigma\in K}\phi_\sigma^K\Big)=\sum_K\sum_{\sigma\in K}\varphi(\sigma)\phi_\sigma^T$$
$$=\int_\Omega\varphi^h\ \text{div}\ f(u^h)dx+\sum_K\Big(\sum_{\sigma\in K}\varphi(\sigma)(\phi_\sigma^K-\phi_\sigma^{K,c})\Big)$$

The next step is to see that $\sum_{\sigma\in K}\phi_\sigma^{T,c}=\phi^K$ so that we have

$$\sum_{\sigma\in K}\varphi(\sigma)(\phi_\sigma^K-\phi_\sigma^{K,c})=\frac{1}{n_K!}\sum_{\sigma,\sigma'\in K}(\phi(\sigma')-\phi(\sigma))(\phi_\sigma^K-\phi_\sigma^{K,c})$$

Then, we make the following remark: if the exact solution of *steady* version (13) is smooth enough, then for any σ and K

$$\phi_\sigma^K(w^h)=O(h^{k+d})\ \text{and}\ \phi^K(w^h)=O(h^{k+d}).$$

Let us look at the first relation. The second one is the sum of the first ones. We have

$$\begin{aligned}\phi_\sigma^K(w^h)&=\int_K\psi_\sigma\ \text{div}\ f(w^h)dx\\&=\int_K\psi_\sigma\ \text{div}\ \Big(f(w^h)-f(u)\Big)dx\\&=\int_{\partial K}\psi_\sigma\Big(f(w^h)-f(u)\Big)\cdot\vec{n}dx-\int_K\nabla\psi_\sigma\Big(f(w^h)-f(u)\Big)\\&=O(h^{d-1})\times O(h^{k+1})+O(h^d)\times O(\frac{1}{h})\times O(h^{k+1})\\&=O(h^{k+d})\end{aligned}$$

To get the second line, we explicitly use the fact that $\int_K\psi_\sigma\ \text{div}\ f(u)dx=0$ because the problem is steady, the second line comes from the Gauss theorem, the third line use that fact that f is Lipschitz continuous, $w^h-u=O(h^{k+1})$ and the regularity assumption of the mesh.

Thanks to this, we see that

$$\int_\Omega\varphi^h\text{div}\ f(w^h)=O(h^{k+1})$$

and

$$\sum_K\Big(\sum_{\sigma\in K}\varphi(\sigma)(\phi_\sigma^K-\phi_\sigma^{K,c})\Big)=O(h^{k+1})$$

if $\phi_\sigma^K=O(h^{k+d})$ again if the mesh is regular. Indeed, we have

$$\mathcal{E}'=\sum_K\Big(\sum_{\sigma\in K}\varphi(\sigma)(\phi_\sigma^K-\phi_\sigma^{K,c})\Big)$$
$$=N_K\times n_K\times O(\nabla\varphi)\times h\big(\times O(\phi_\sigma^K)+O(\phi_\sigma^{K,c})\big)$$

The mesh is regular so that the number N_K of elements is $O(h^{-d})$, n_K is fixed, $O(\phi_\sigma^{K,c})=O(h^{k+d})$ and $\phi_\sigma^K=O(h^{k+d})$, hence

$$\mathcal{E}'=O(h^{-d})\times O(h)\times O(h^{k+d})=O(h^{k+1}).$$

This shows that if $\phi_\sigma^K = O(h^{k+d})$ then

$$\mathcal{E}_h(u) \leq Ch^{k+1}$$

and the scheme is (formally) $k+1$-th order accurate.

This analysis leads to residuals of the form

$$\phi_\sigma^K = \beta_\sigma^K \phi_K \tag{18}$$

where the family $\{\beta_\sigma^K\}_{\sigma,K}$ is uniformly bounded when $h \to 0$. In the next paragraph, we discuss the construction of scheme of the form (18) that are both formally high order accurate *and* L^∞ stable. In many cases, one can see experimentally that the schemes (18) are over-compressive. This can be cured if one adds dissipation. This can be done without violating (17) by adding a selected form of dissipation, namely

$$\phi_\sigma^K = \beta_\sigma^K \phi_K + \theta h_K \int_K \big(\nabla_u f(u^h)\cdot\nabla\psi_\sigma\big)\tau\big(\nabla_u f(u^h)\cdot\nabla u^h\big)dx \tag{19}$$

where θ is a positive parameter. This form of dissipation is reminiscent of the stabilization term of the SUPG scheme [19] but here, as shown later, it plays the role of filter. In practice, the positive parameter τ is set to

$$\tau = \left(\sum_{\text{i: vertices of K}} \max(\nabla_u f(\overline{u^h})\nabla\Psi_i, 0)\right)^{-1}. \tag{20}$$

In (20), we only consider the vertices of K, and the Ψ_is are the lowest order finite element constructed on K : linear polynomials for triangles and tets, Q^1 for quads and hex, etc. Last $\overline{u^h}$ is the arithmetic average on the degrees of freedom in K.

Remark 4.2 (About the effective accuracy)**.** *In practice, we are never able to exactly satisfy* (15c) *for any degree of freedom, but*

$$\sum_{K,\sigma\in K} \phi_\sigma^K(u^h) = \varepsilon_\sigma \tag{21}$$

The previous truncation error analysis leads to

$$\mathcal{E}_h(u) \leq Ch^{k+1} + \sum_K \varepsilon_\sigma$$

ans the same analysis shows that we need to have

$$\max_\sigma |\varepsilon_\sigma| = O(h^{k+d+1}). \tag{22}$$

4.1.6 Getting both accuracy and stability.

All the known RD schemes have the form

$$\phi_\sigma^K = \sum_{\sigma'\in K} c_{\sigma\sigma'}(u_\sigma - u'_\sigma).$$

It is well known that if $c_{\sigma\sigma'} \geq 0$, and if a solution of (15) exists, it satisfies a maximum principle. Hence, we are going to construct schemes of the form (18) with positive $c_{\sigma\sigma'}$. This is done in two steps.

- First step. We construct a family of sub-residuals that ensures first order accuracy and stability in L^∞. The simplest choice is an extension of the local Lax Friedrichs scheme:

$$\phi_\sigma^{K,LxF} = \frac{\phi^K}{n_K} + \alpha\big(u_\sigma - \overline{u}_K\big) \tag{23}$$

with

$$\overline{u} = \frac{\sum_{\sigma\in K} u_\sigma}{n_K} \text{ and } \alpha \geq \max_K ||\nabla_u f(u^h)||.$$

These choices guaranty that the scheme is L^∞ stable, and more precisely we have

$$c_{\sigma\sigma'} = \frac{1}{n_K}\left(\int_T \nabla_u f(u^h)\cdot\nabla\psi_{\sigma'}dx + \alpha\right)$$

- We define $(\phi_\sigma^K)^\star = \beta_\sigma^K \phi^K$ with

$$\beta_\sigma^K = \frac{\max(0, \frac{\phi_\sigma^{K,LxF}}{\phi_K})}{\sum\limits_{\sigma'\in K}\max(0, \frac{\phi_{\sigma'}^{K,LxF}}{\phi_K})}. \tag{24}$$

This is one of the many choices that guaranties $(\phi_\sigma^K)^\star = \sum_{\sigma'\in K}\widetilde{c}_{\sigma\sigma'}(u_\sigma - u_{\sigma'})$ with $\widetilde{c}_{\sigma\sigma'}\geq 0$. It is constructed following:

$$(\phi_\sigma^K)^\star = \frac{(\phi_\sigma^K)^\star}{\phi_\sigma^{K,LxF}}\phi_\sigma^{K,LxF} \sum_{\sigma'\in K}\frac{(\phi_\sigma^K)^\star}{\phi_\sigma^{K,LxF}}c_{\sigma\sigma'}^{LxF}(u_\sigma - u_{\sigma'})$$

Then we set $\widetilde{c}_{\sigma\sigma'} = \frac{(\phi_\sigma^K)^\star}{\phi_\sigma^{K,LxF}}c_{\sigma\sigma'}^{LxF}$ which is positive if (and only if) $(\phi_\sigma^K)^\star \times \phi_\sigma^{K,LxF}\geq 0$ that is,

$$\beta_\sigma^K\frac{\phi_\sigma^{K,LxF}}{\phi_K}\geq 0.$$

The relation (24) is obtained by satisfying these relations for any $\sigma\in K$.

4.2 Extension to systems.

In the case of systems,

$$\text{div } \mathbf{f}(\mathbf{u}^h) = 0$$

the generalization is straightforward: no modification is needed except the way the coefficients β_σ^K is evaluated. We first note that since ϕ_K and ϕ_σ^{LxF} are vectors, the construction (24) is meaningless. This is why we rely on a characteristic decomposition of the total and sub-residuals. More precisely, we consider a direction $\vec{d}$, the left and right eigen-vectors of $K_{\vec{d}} := \nabla\mathbf{f}(\overline{\mathbf{u}})\cdot\vec{d}$. They are denoted, respectively, by $\{\mathbf{r}_\xi\}_{\xi \text{ eigenvalues of A}}$ and $\{\ell_\xi\}_{\xi \text{ eigenvalues of } K_{\vec{d}}}$. By construction, we have $\ell_\xi(\mathbf{r}_{\xi'}) = \delta_\xi^{\xi'}$.

Consider a set of first order residuals $\{\phi_\sigma^{K,L}\}_{\sigma\in K}$ with

$$\sum_{\sigma\in K}\phi_\sigma^{K,L}=\phi_K=\int_{\partial K}\mathbf{f}(\mathbf{u}^h)\cdot\vec{n}dl.$$

An example is given by the Lax Friedrichs residuals,

$$\phi_\sigma^{K,LxF}=\frac{1}{n_K}\phi_K+\alpha_K(u_\sigma-\overline{u})\qquad\text{with }\overline{u}=\frac{1}{n_K}\sum_{\sigma\in K}u_\sigma.$$

We decompose the residuals $\phi_\sigma^{K,L}$ onto the eigenbasis,

$$\phi_\sigma^{K,L}=\sum_{\xi\text{ eigenvalues of }K_{\vec{d}}}\ell_\xi\big(\phi_\sigma^{K,L}\big)\mathbf{r}_\xi \tag{25a}$$

By construction, we have, for any ξ,

$$\sum_{\sigma\in K}\ell_\xi\big(\phi_\sigma^{K,L}\big)=\ell_\xi\big(\phi_K\big) \tag{25b}$$

and we remark that the characteristic $\ell_\xi\big(\phi_\sigma^{K,L}\big)$ are scalar quantities. We can apply the same technique as in the scalar case to them. For example, using (24), we define

$$\ell_\xi\big(\phi_\sigma^{K,L}\big)^\star=\beta_\sigma^{K,\xi}\ell_\xi\big(\phi_K\big) \tag{25c}$$

and then the high order residuals are

$$\phi_\sigma^{K,\star}=\sum_{\xi\text{ eigenvalues of }K_{\vec{d}}}\ell_\xi\big(\phi_\sigma^{K,L}\big)^\star\mathbf{r}_\xi. \tag{25d}$$

The last step, as in the scalar case, is to add a dissipation term, as in (19). By analogy, the final residual is

$$\phi_\sigma^K=\phi_\sigma^{K,\star}+\theta h_K\int_K\nabla\psi_\sigma\tau\nabla_u f(u^h)\cdot\nabla u^h dx \tag{25e}$$

The matrix τ is constructed by analogy to (20), namely

$$\tau=\left(\sum_{\text{i: vertices of K}}\max(\nabla_u f(\overline{u^h})\nabla\Psi_i,0)\right)^{-1} \tag{25f}$$

and again $\overline{u^h}$ is the arithmetic average of the solution over the degrees of freedom and $\max(A,0)$ is the positive part of the matrix A which is assumed to be diagonalisable in $\mathbb{R}$ with real eigenvalues.

We have left unclear the choice of $\vec{d}$. In practice, we choose $\vec{d}=\vec{u}/||\vec{u}||$ and an arbitrary direction if $\vec{u}=0$. The many experiments we have conducted shows that the non oscillatory behavior of the scheme is independant of the choice of $\vec{d}$. Of course for any direction choice will correspond a particular scheme, but all have the same non oscillatory behavior. The specific choice is motivated by keeping the rotational invariance of the scheme.

4.2.1 Boundary conditions.

We have used a simplified version of the boundary conditions. If an element K has an edge, Γ_K, on the boundary, we need to add to the degrees of freedom on Γ_K a boundary residual. We denote it by $\Phi_\sigma^{\Gamma_K}$. These residuals should satisfy the conservation relation

$$\sum_{\sigma\in\Gamma_K} \Phi_\sigma^{\Gamma_K} = \int_{\Gamma_\sigma} \big(\mathcal{F}_n(u^h) - f(u^h)\cdot\vec{n}\big)dl$$

where $\mathcal{F}_n$ is a boundary flux. In the examples of this paper, two types of boundary are considered:

- *Wall boundary conditions* . The condition $\vec{u}\cdot\vec{n}=0$ is weakly imposed so that
$$\mathcal{F}_n(u^h) = \begin{pmatrix} 0 \\ p(u^h)n_x \\ p(u^h)n_y \\ 0 \end{pmatrix}$$
- *Inflow/outflow boundary conditions.* The state at infinity is U_∞ and we take here the modified Steger-Warming flux
$$\mathcal{F}_n(u^h) = \big(A(u^h)\cdot\vec{n}\big)^+ u^h + \big(A(u^h)\cdot\vec{n}\big)^+ u_\infty.$$

By analogy with what is done in [1], we have chosen a 'centered' version of the boundary residuals, namely

$$\Phi_\sigma^{\Gamma_K} = \int_{\Gamma_K} \big(\mathcal{F}_n(u^h) - f(u^h)\cdot\vec{n}\big)\psi_\sigma(x)dl$$

where again ψ_σ is the Lagrange basis function defined in K for σ. This is approximated by a quadrature formula with positive weights. The quadrature formula should be of order $k+d-1$, i.e. 3 for a third order scheme in 2D. The actual residual is

$$\Phi_\sigma^{\Gamma_K} = |\Gamma_K| \sum_{\text{quadrature points}} \omega_{quad}\big(\mathcal{F}_n(u^h) - f(u^h)\big)(x_{\text{quad}})\cdot\vec{n}. \qquad (26)$$

In the case of interest ($\mathbb{P}^2/\mathbb{Q}^2$ interpolation), we approximate these relation with Simpson's formula : only one term appears in the sum and it corresponds to σ.

All the meshes we have used are made of triangles or quadrangles. We have used two type of boundary representation. In the first one we adopt a piecewise linear representation of the boundary but we might be quite far from the true geometry. In the second representation, we use a quadratic representation of the geometry. In principle, the situation should be better, but one has to be aware of two difficulties. First, the "numerical" representation of the boundary is not C^1 in general, even if the boundary is C^∞. An example is provided on figure 2 where we approximate the boundary of a NACA012 airfoil near the symmetry axis. The second problem is that even very simple geometries, such as circle, will not be represented exactly.

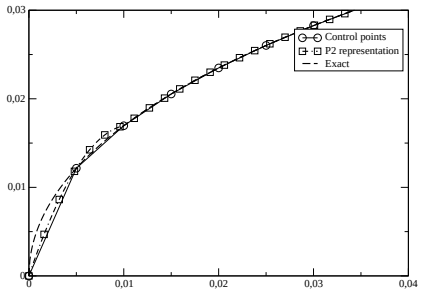

Figure 2: Comparison with the true geometry between the two boundary representation methods used in this paper. The degrees of freedom are represented by circles.

The second drawback could be solved by using NURBS representation of the boundary, see section 6, the first one is here solved as follows: instead of trying to interpolate *exactly* in each boundary segment the boundary curve, we use a Bézier representation which amount to interpolate at the boundary points and respect the tangents at these points. We get an approximate quadratic representation of the boundary. This is the method we have used in practice.

In order to simplify the coding, we have used use an isoparametric representation of each element, even for the interior elements. The filtering operator is the adapted to this context : we need a exact evaluation of the gradient and divergence operators.

5 Numerical examples.

We illustrate the previous paragraph by numerical examples.

5.1 Role of the filtering parameter.

We start with the advection problem with initial states and advection speeds defined by

$$\vec{\lambda} = (1,2)^T \quad \text{and } u(x,y) = \begin{cases} 1 & \text{if } x = 0 \text{ and } y > 0 \\ 0 & \text{if } y = 0 \text{ and } x > 0 \end{cases} \tag{27}$$

The second problem is obtained by setting

$$\vec{\lambda} = (y,-x)^T \quad \text{and} \quad u(x,y) = \begin{cases} \varphi_0(x) & \text{if } y = 0 \\ 0 & \text{otherwise} \end{cases} \tag{28}$$

where

$$\varphi_0(x) = \begin{cases} \cos^2(2\pi x) & \text{if } x \in [0.25, 0.75] \\ 0 & \text{else} \end{cases}$$

The meshes are made of triangles, but this is not essential in the discussion. The figures 4 show the solution obtained for (27) and (28) by the scheme using $\mathbb{P}^2$ element *without* the term (19), while the figure 6 show the same results with (19). The problem (27) is well resolved without the τ term as it can be seen on

figure 4, top-left, but the cross-section (top-right) shows that the solution looks wiggly in the discontinuity. This is not an instability mechanism, since we can show that the scheme is perfectly stable in the L^∞ norm. The same comments can be done on the solution of problem (28), which, a priori, should be simpler : it is a smooth solution. In fact the situation looks even worse. We emphasis again on the fact that these "wiggles" are not a manifestation of an instability mechanisms. In fact, the scheme appears too compressive, and in [5], we give an heuristic explanation of the cause of this phenomenon.

We can show that the scheme without the term (19) will *always* have this problem. To do this, we have a very simple counter example. We consider $\Omega = [0,1]^2$ which is discretised by uniform quads. The vertices are $x_{i,j} = (\frac{i}{N}, \frac{j}{N})$ $(0 \leq i,j \leq N)$ and the problem writes

$$\frac{\partial u}{\partial x} = 0$$

subjected to boundary conditions on the left side of Ω. Assuming a general scheme of the form $\phi_\sigma^K = \beta_\sigma^K \phi^K$, we update the solution by

$$u_\sigma^{n+1} = u_\sigma^n - \omega\Big(\sum_{K,\sigma\in K} \beta_\sigma^K \Phi^K\Big)$$

Two things need to be precised : the boundary conditions and the initial state u^0. On the left boundary (inflow), we impose a check-board like mode, but this is not really essential as we see at the end of the paragraph), i.e.

$$u_\sigma = (-1)^{i_\sigma}$$

where i is the index such that $\mathbf{x}_\sigma = (\frac{i}{N}, 0)$ and $u_\sigma = 0$ is σ is any mid point. The initial condition is defined by

- either as on figure 5-a : we "propagate" the boundary condition along the characteristics of the PDE.
- or as on figure 5-b.

We expect to converge to the first initialization. Let us compute the total residual on $Q = [x_i, x_{i+1}] \times [y_j, y_{j+1}]$. We get

$$\Phi^Q = \int_{y_j}^{y_{j+1}} \int_{x_i}^{x_{i+1}} \frac{\partial u}{\partial x} dxdy = \int_{y_j}^{y_{j+1}} \big(u(x_{i+1},y) - u(x_i,y)\big)dx.$$

In our case, we have, by symmetry, $u(x_{i+1},y) = u(x_i,y)$, so that $\Phi^Q = 0$ and $u_\sigma^{n+1} = u_\sigma^n$. This shows that the scheme cannot converge in this case .... Hence, something more must be done !

Let us come back to the numerical examples, and in particular the results of figure 6 where (19) has been added. One concern is that when adding (19), the scheme do not any longer preserve the maximum prionciple. The left picture of figure 6 shows that, for the discontinuous solution of problem (27), we do not get any spurious oscillations. The right picture instead shows, for problem (28), the

positive effect of the extra term in smoothing the contours that now are perfectly circular. We have also run a grid refinement study on this problem using $\mathbb{P}^2$ and $\mathbb{P}^3$ approximations. The results are summarized on table 1. The slope are obtained by least squares fitting, this confirms the expected convergence rates.

To better visualize the improvement in the solution when going from $\mathbb{P}^1$ to $\mathbb{P}^2$ spatial interpolation, we consider, on the spatial domain $[0,2]\times[0,1]$, the solid body rotation of the inlet profile $u(x)=\sin(10\pi x)$. In this case the advection speed is set to $\vec{\lambda}=(y,1-x)$. Note that the $\mathbb{P}^1$ run has been performed on the mesh obtained by sub-triangulating the $\mathbb{P}^2$ mesh so that exactly the same number of DOF is used in the two cases. The dramatic improvement brought by the $\mathbb{P}^2$ approximation is clearly visible in the contour plots, and also in the outlet profiles reported on figure 3.

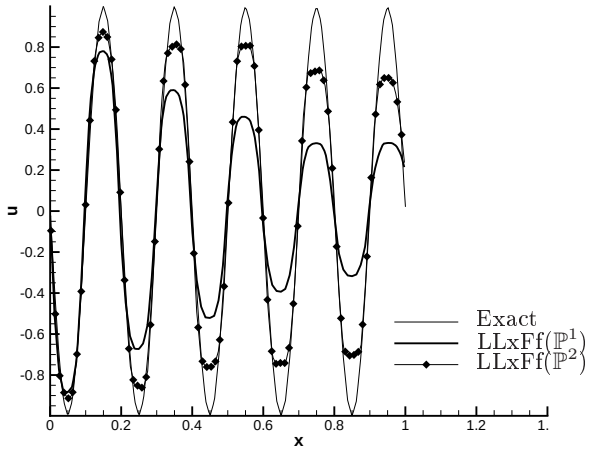

Figure 3: Rotation of the smooth profile: $u_{\text{in}}=\sin(10\pi x)$. Computed outlet profile. All computations run on the same number of degrees of freedom. Reference mesh size $h=1/80$.

We test further the behavior of (19)-(24) by solving the 2D Burgers's problem

$$\frac{\partial u}{\partial y}+\frac{1}{2}\frac{\partial u^2}{\partial x}=0 \qquad \text{if } x\in[0,1]^2$$
$$u(x,y)=1.5-2x \qquad \text{on } y=0.$$

The exact solution consists in a fan that merges into a shock which foot is located at $(x,y)=(3/4,1/2)$. More precisely, the exact solution is

$$u(x,y)=\begin{cases} \text{if } y\geq 0.5 & \begin{cases} -0.5 & \text{if } -2(x-3/4)+(y-1/2)\geq 0 \\ 1.5 & \text{else} \end{cases} \\ \text{else} & \max\left(-0.5,\min\left(1.5,\dfrac{x-3/4}{y-1/2}\right)\right) \end{cases}$$

The results obtained on the mesh of figure 4 are displayed on figure 7. For the sake of comparison, we give the second and third order results on the same mesh (hence the $\mathbb{P}^2$ results have more degrees of freedom).

We note that there are no spurious oscillation across the shock. We had the same conclusions on all the test case we have run, even in the non convex case. This indicates that though the term (19) prevent a formal maximum principle, its role is very different to what it is in a SUPG like scheme: it only filters spurious modes, has no role in the stability and helps to converge the iterative scheme so that the error in (21) really behaves like (22).

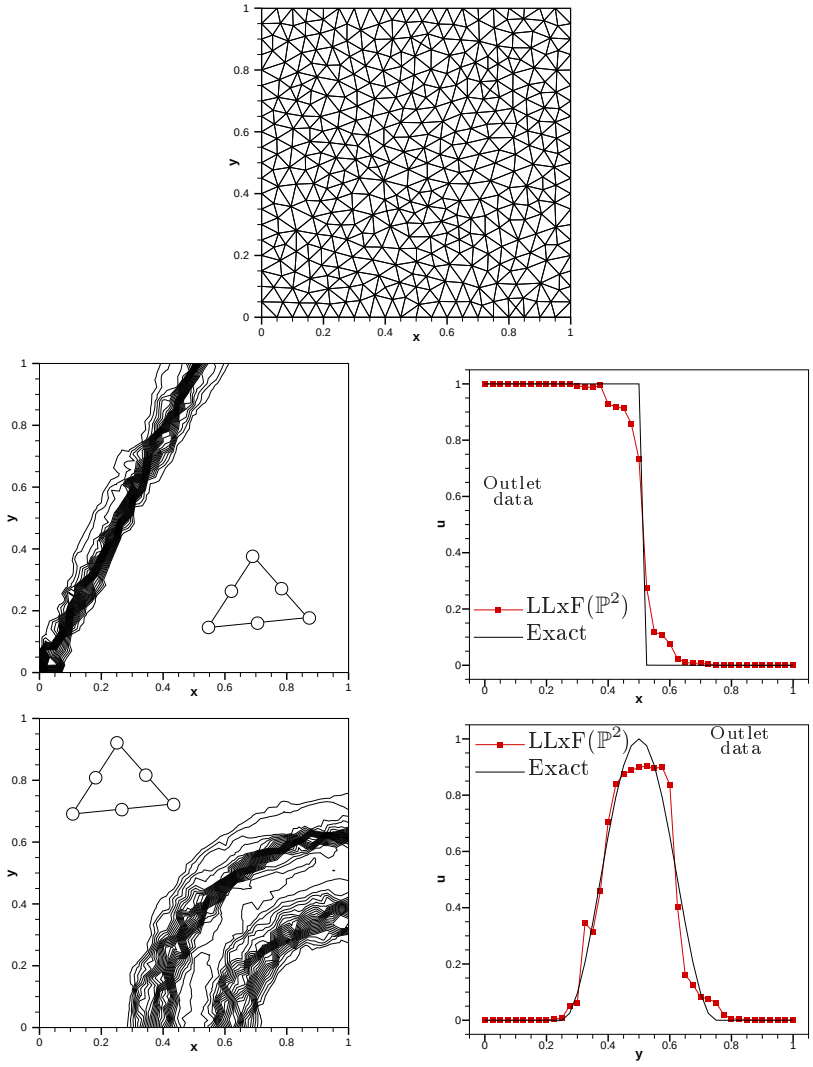

Figure 4: Convection problem : Results obtained with scheme (18)–(24) for $\mathbb{P}^2$ interpolation. Top : mesh. Middle : result for problem (27). Bottom : results for problem (28). The first order scheme is (23).

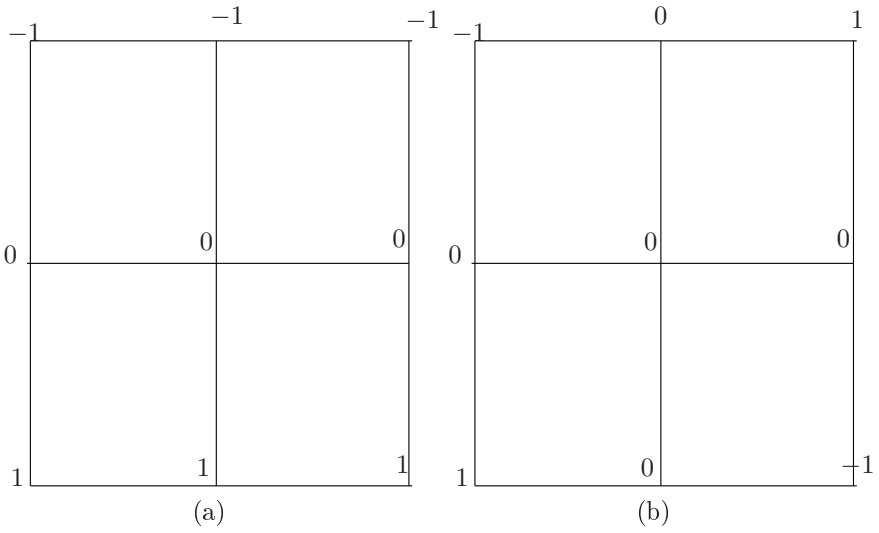

Figure 5: Two initializations showing the creation of spurious modes. We show an elementary quad. The global initialization is obtained by reproducing periodically the pattern.

h	$\epsilon_{L^2}(P^1)$	$\epsilon_{L^2}(P^2)$	$\epsilon_{L^2}(P^3)$
1/25	0.50493E-02	0.32612E-04	0.12071E-05
1/50	0.14684E-02	0.48741E-05	0.90642E-07
1/75	0.74684E-03	0.13334E-05	0.16245E-07
1/100	0.41019E-03	0.66019E-06	0.53860E-08
	$\mathcal{O}^{\text{ls}}_{L^2}$ =1.790	$\mathcal{O}^{\text{ls}}_{L^2}$ =2.848	$\mathcal{O}^{\text{ls}}_{L^2}$ =3.920

Table 1: L^2 errors for (28)–(27) with $u(x) = \varphi_0(x)$ on the inflow.

5.2 Compressible flow examples.

We have run many test cases ranging from low subsonic, subsonic, transonic to supersonic flows. We only select two cases: one subsonic flow where we show the behavior of the scheme depending on the mesh structure and a supersonic one. In the latter case, the concern is not in the accuracy but on the robustness of the scheme since the solution presents very complex waves interactions.

5.2.1 Subsonic flows.

We have run the case of a flow at $M_\infty = 0.35$ over a sphere. In that case, the flow is symmetric with respect to the x–axis of the domain, but also with respect to the y axis. The flow stays subsonic, so that an easy accuracy criteria is the behavior of the entropy. We have run this case with a second order scheme, a third order scheme, and again the second order scheme on the mesh that has the same degrees of freedom as those of the $\mathbb{P}^2$ scheme. In other words, we subdivide each triangle into 4 smaller triangles which vertices are those of the

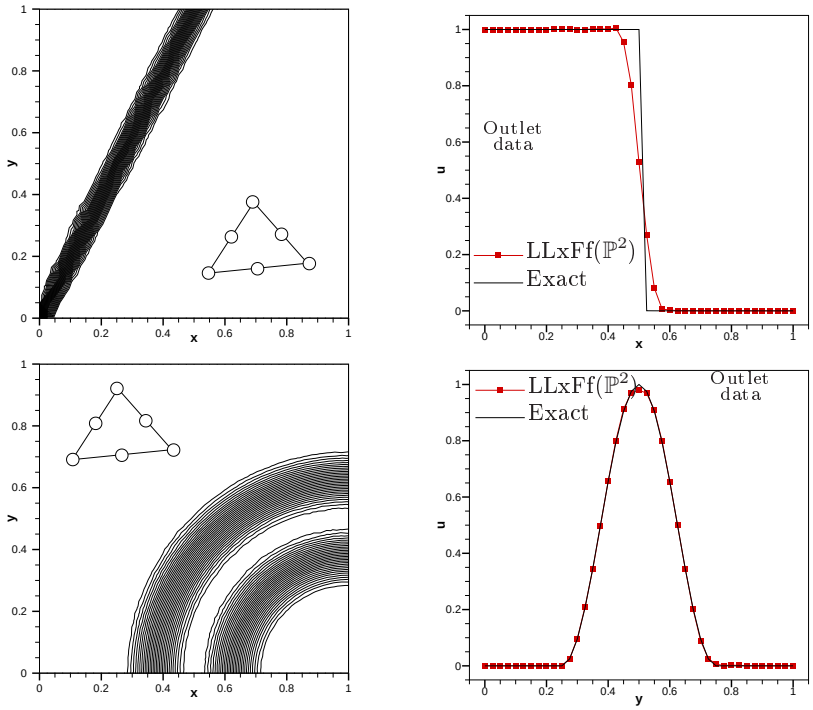

Figure 6: Rotation problem : Results obtained with the scheme (19)–(24) for $\mathbb{P}^2$ interpolation. Top : result for problem (27) (min $= -1.0094$, max $= 1.01$). Bottom : results for problem (28) (min $= -0.1735\,10^{-4}$). The first order scheme is (23).

large triangle and the mid–edges points. The initial mesh has 2719 nodes, 5308 elements and 100 nodes on cylinder. It is displayed on figure 8.

We see on figure 9 which displays the pressure coefficient isolines the improvement of the solution quality when the scheme is upgraded from second order to third order. More important, the same figure indicates clearly that the second order scheme on the refined mesh gives less accurate results than the third order one. Note that we have the same degrees of freedom in both cases.

This result is confirmed by Figure 10 which displays the entropy variation along the boundary. Except at the forefront stagnation point, the entropy deviation of the third order scheme is much closer than the exact one.

We have re-run this test case on an hybrid mesh using the second order and the third order schemes. In both cases, the same degrees of freedom are used (i.e. we use the dofs of the sub-triangulation for the second order scheme). The results are shown on figure 11. The mesh use 81 points on the sphere. We get the same conclusions as before.

5.2.2 Scramjet.

We have run the same scheme on a scramjet–like configuration using an hybrid mesh as shown on figure 12. The inflow mach number is set to 3.5. The geometry

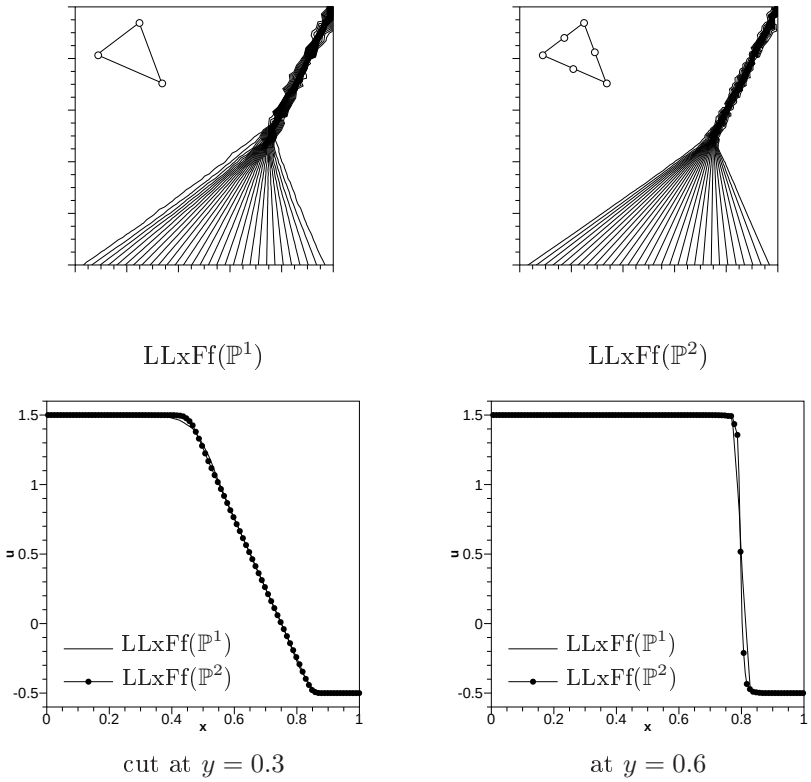

Figure 7: Burger equation, solution obtained with a $\mathbb{P}^1$ and $\mathbb{P}^2$ Lagrange interpolated and the scheme (19)-(24).

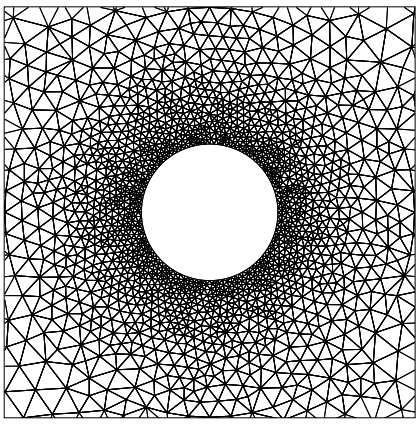

Figure 8: Subsonic sphere problem : Zoom of the mesh for the sphere problem. The mesh has no symetry.

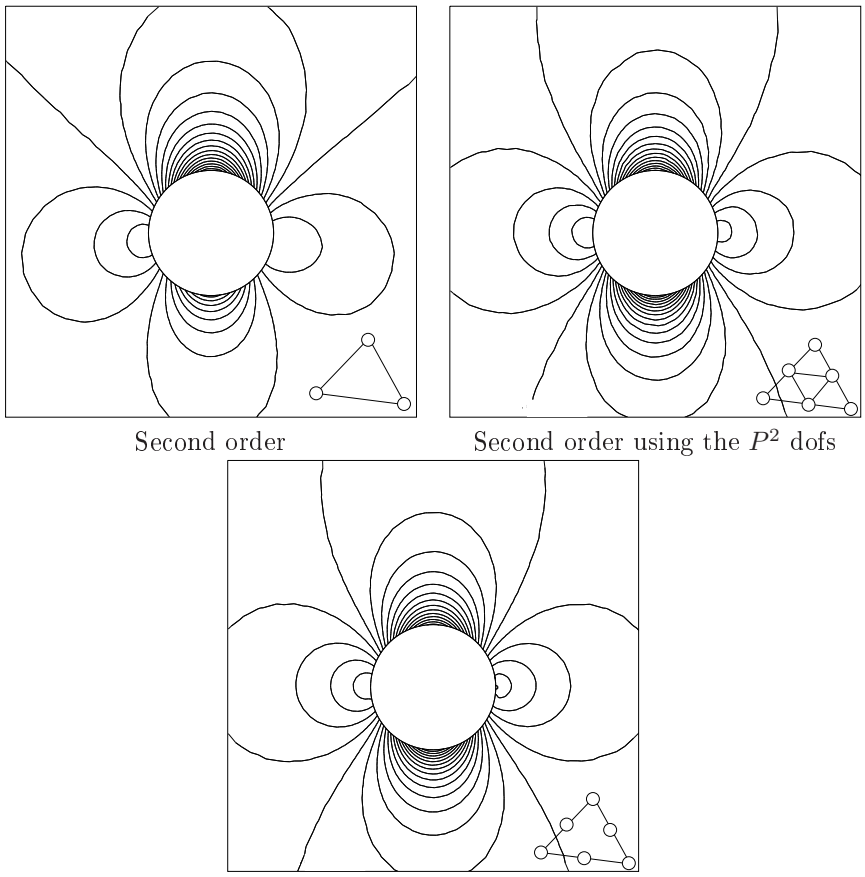

Figure 9: Subsonic sphere problem : Isolines of the pressure coefficient. We have the same isolines on each figure.

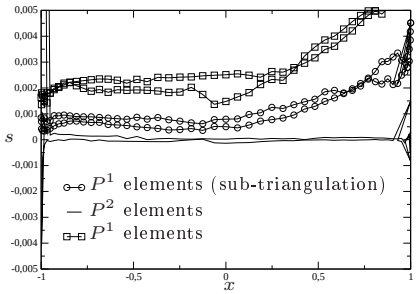

Figure 10: Subsonic sphere problem : Entropy variation along the boundary.

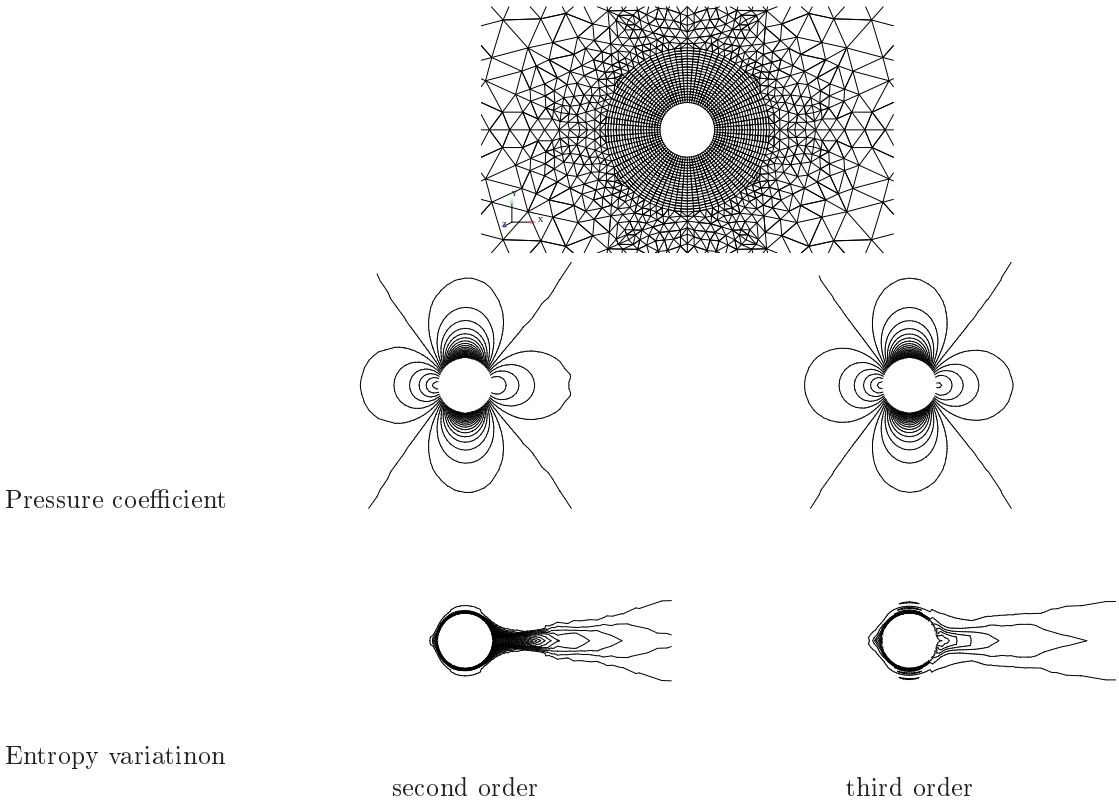

Figure 11: Subsonic sphere problem, hybrid mesh : Pressure coefficient and entropy variation on an hybrid mesh, $M_\infty = 0.35$.

is such that many waves coexist and interact in very complex flow patterns. This situation is particularly clear on the upper part of the internal body where shocks, fans and their reflection due to wall interact. Again, in both cases, the same number of degrees of freedom have been used. Once again, the scheme has been run starting from a uniform flow configuration. figure 13 shows the Mach number isolines. As expected, there is no real difference between the solutions since the flow is basically made of shock, fans, slip lines and constant states : this is not an accuracy case, but a case that shows that, despite the flow complexity, the third order scheme is robust.

However, one can see a small difference between the solutions : the slip line created by the interaction of two shocks after the blade is a little bit more twisted for the third order scheme than the second order one. We also see that the resolution of the discontinuities is in both case approximately one cell width.

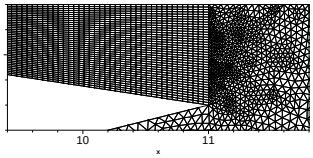

Figure 12: Zoom of the mesh for the Scramjet problem.

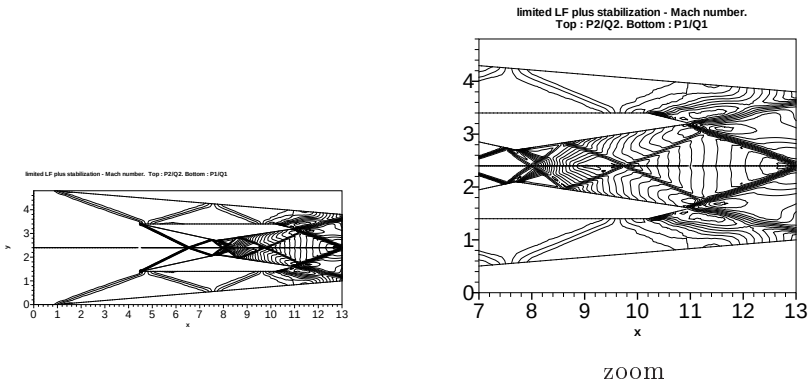

Figure 13: Scramjet problem. Mach number distribution. Top : the third order solution, bottom the second order solution. The same isolines are plotted.

6 Extensions.

This method can be extended along several directions: unsteady problems, a more complex model such as the (laminar) Navier Stokes equations, different models such as the Shallow water system (see [26] for an extension of the second order scheme for problems including dry beds), or the MHD equations [4]. We quickly cover the unsteady case and the viscous problems.

6.1 Unsteady problems.

As seen above, the main reason why the schemes can reach arbitrary order of accuracy is because the residual behave, in the case of a smooth enough solution, like

$$\phi_\sigma^K(w^h) = O(h^{k+d})$$

where d is the physical dimension and k the expected order of accuracy. To get this behavior, there are two key ingredients

- the interpolation of the smooth solution of the problem is of order $k+1$,
- we run a steady problem: the fact that

$$\int_{\partial K} f^h(u^h) \cdot \vec{n} dl = 0$$

  for any element plays a central role.

Because of that, one cannot extend these schemes to unsteady problems via a time/space splitting approach. If this is done, one only get first order accuracy : we need to introduce the structure of the PDE, div $f(u^h) = 0$ somewhere, somehow, in the numerics.

The first natural idea is to consider the time/space problem

$$\frac{\partial u}{\partial t} + \text{ div } f(u^h) = 0$$

as a whole. In the RD approach, this has been done by [10, 27, 15] to give a few examples. This leads to implicit schemes with possibly stability constraints. These stability constraints can be removed by a "two-layers" technique, see [27] and then [10] for details. A simpler method is described in [15], it uses discontinuous in time finite elements.

The second natural idea is to "pre-discretise" in time, as it is standard in finite element methods. For example, second order accuracy can be reached either by starting from a Crank-Nicholson scheme

$$\frac{u^{n+1}-u^n}{\Delta t} + \frac{1}{2}\Big(\text{ div } f(u^n) + \text{ div } f(u^{n+1})\Big) = 0$$

or a BDF-like approach

$$\frac{3}{2}\frac{u^{n+1}-u^n}{\Delta t} - \frac{1}{2}\frac{u^n-u^{n-1}}{\Delta t} + \text{ div } f(u^{n+1}) = 0.$$

In both cases, we end up to solving a problem of the form

$$\alpha v + \text{ div } f(v) - S(x) = 0$$

where $v := u^{n+1}$, $\alpha = 1/\Delta t$ in the Cranck Nicholson case and $\alpha = \frac{3}{2\Delta t}$ in the BDF case. The only difference with the previous case is the definition of the total residual. It is naturally

$$\phi^K = \int_K \big(\alpha v - S(x)\big) dx + \int_{\partial K} f(u^h) \cdot \vec{n} dx$$

The inclusion of the source term in the total residual is dictated again by accuracy considerations. This approach has been considered in [3], then extended to flow problems (unpublished).

A much more interesting approach, because it is explicit and very cheap, as well as needing very little modifications of the computer code has been proposed in [24], only for second order space-time schemes so far with triangular meshes. One example of such scheme for

$$\frac{\partial u}{\partial t} + \text{ div } f(u^h) = 0$$

is: Starting from $v^0 := u^n$

1. First step. One evaluates v^1 by the scheme

$$|C_\sigma| \frac{v^1_\sigma - v^0_\sigma}{\Delta t} + \sum_{\sigma \in T} \psi^T_\sigma(v^0) = 0$$

with

$$\psi^T_\sigma(v^0) = \beta^T_\sigma(v^0) \int_{\partial T} f(v^0) \cdot \vec{n} dl.$$

We note that in the $\mathbb{P}^1$ case, the filtering term can also be written as $\gamma^T_\sigma \int_{\partial T} f(v^0) \cdot \vec{n} dl$, this is why the previous relation can cover all cases.

2. Second step. Knowing v^0 and v^1, we define v^2 as

$$|C_\sigma| \frac{v^2 - v^1}{\Delta t} + \sum_{\sigma \in T} \beta^T_\sigma(v_0, v^1) \psi^T_\sigma(v^0, v^1) = 0$$

with

$$\psi^T_\sigma(v^0, v^1) = \int_K \frac{v^1 - v^0}{\Delta t} + \int_{\partial K} f(u^h) \cdot \vec{n} dl.$$

The scheme is fully explicit. In [24], a full analysis is conducted, other schemes are presented. We pick out one result, that of the Mach 10 DMR test case [34], to illustrate the results, see figure 14.

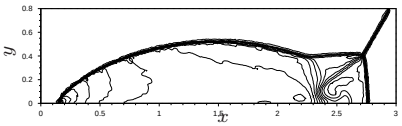

Figure 14: Double Mach reflection. Density contours. 30 equally spaced contours from 1 to 24. Taken from [24].

6.2 Viscous problems.

6.2.1 A simple formulation.

This topic is also the subject of current active research. Let us write the (steady) system as

$$\text{div } (F_e - F_v) = 0 \tag{29}$$

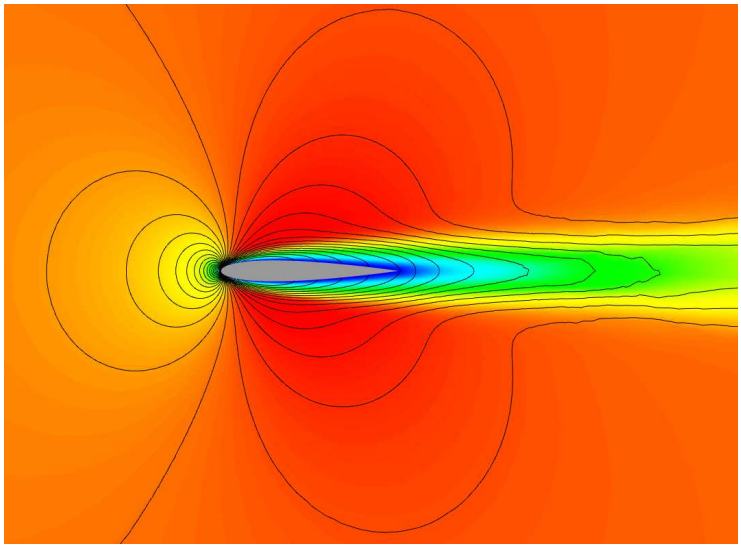

Figure 15: Third order solution on the finest mesh for the steady viscous NACA012 test case. x-velocity in color and isolines of the density component.

with standard boundary conditions. F_e are the standard Euler fluxes and F_v the viscous ones. In A. Larat's PhD thesis, [21], the system (29) has been discretised in two steps. In the first step, the Euler fluxes are approximated using the method of section 4, and in the second one the viscous fluxes are approximated by a Galerkin variational formulation.

This strategy has already been used in previous works on viscous RD schemes with some refinements when the Peclet becomes small since the viscous effects are predominant, see [25]. A formal justification of the method, in the $\mathbb{P}^1$ case, can be found in [9] or in the section 6.2.2.

The approach of [21] is working rather fine (except there is no real theoretical background to this positive result ...). To show this we take a viscous NACA012 airfoil with 0° of incidence, the Mach number at infinity is 0.5 and the Reynolds number is 500. The figure 15 represents the isolines of density colored by the x- component of the velocity. The figure 16 provide the convergence history for the lift. The meshes range from 609 to 230×10^3 vertices. The slope -3 is also represneted.

The results are encouraging but a better and more motivated approach is needed. The next section is devoted to a discussion about what can be done in the RD framework to approximate viscous problems.

6.2.2 Analysis

We are interested in the approximation of convection diffusion problems such as

$$\begin{array}{ll} \text{div } f(u) = \varepsilon \Delta u & x \in \Omega \\ u = g & \text{on } \partial\Omega \end{array} \tag{30}$$

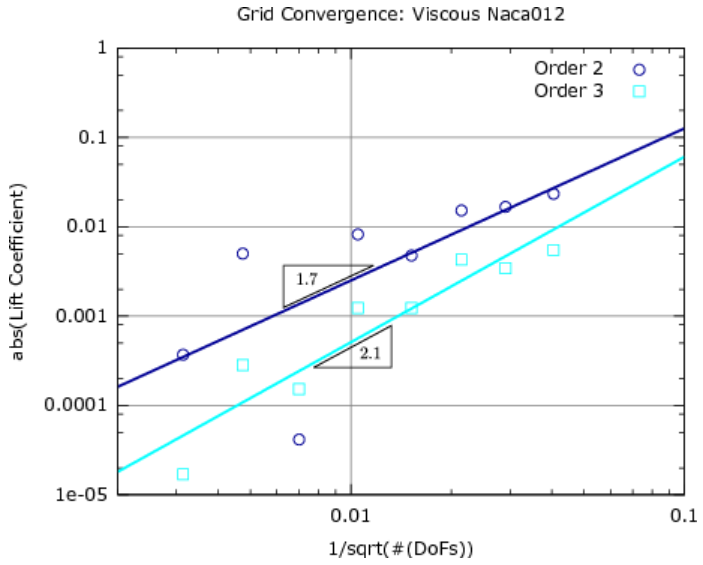

Figure 16: Convergence of the lift coefficient with respect to the mesh characteristic size $h = \sqrt{\#\{\text{dofs}\}}$ for second and third order simulation of the viscous NACA012 problem.

where $f(u)$ is a C^1 function (the flux) and $\varepsilon > 0$. In this section, we would like to illustrate the theoretical difficulties encountered in the scheme of section 6.2.1.

The numerical setting is the following. The domain Ω is triangulated, and to fix ideas, we assume that $\Omega \subset \mathbb{R}^2$ and that the elements of the triangulation $\mathcal{T}_h$ are triangle. None of these two assumptions is essential by any mean.

We first recall a remark of [9] in the $\mathbb{P}^1$ case (second order of accuracy) which shows that the $\mathbb{P}^1$ viscous scase can be seen as standard continuous finite element method where the test functions are spanned by the Lagrange basis function plus bubbles. Then we show, by a counter example, that this remark cannot be extended to higher than second order so that something else has to be done, and is the topic of current research.

Approximation of (30) in the $\mathbb{P}^1$ case. In the $\mathbb{P}^1$ case, and $\varepsilon = 0$, the RD scheme for (30) write: for any mesh point i,

$$\sum_{K \ni i} \phi_i^K = 0 \tag{31}$$

where the residuals are subjected to the conservation condition

$$\sum_{i \in K} \phi_i^K = \phi^K := \int_{\partial K} f(u) \cdot \vec{n} dl \tag{32}$$

where we have introduced the flux $f(u) = \vec{\lambda} u$. In the second order case, the resiudal are of the form

$$\phi_i^K = \beta_i^K \phi^K \tag{33}$$

where $\{\beta_i^K\}$ is uniformly bounded and constructed by various means.

Using the standard shape function φ_i, we can rewrite ϕ^K in a Petrov Galerkin manner,

$$\phi_i^K = \int_K \varphi_i \nabla f(u^h) dx + \int_K (\beta_i^K - \frac{1}{3}) \nabla f(u^h) := \int_K \omega_i^K \nabla f(u^h)$$

because $f(u^h)$ is a linear function and $\int_K \varphi_i dx = |K|/3$. The problem of this formulation is that ω_i is not continuous accross edges, and then cannot be used to approximate (30).

In [9], it was noticed that the same scheme could be written differently. Denote b_K the hat function that is 0 on ∂K and 1 at the gravity center of K. It is a piecewise linear function that enjoys

$$\int_{\partial K} \nabla b^K \cdot \vec{n} dl = 0 \text{ and } \int_K b^K dx > 0.$$

We can write

$$\phi_i^K = \beta_i^K \phi^K = \int_K \varphi_i \nabla f(u^h) dx + \gamma_i^K \int_K b^K \nabla f(u^h)$$

with

$$\gamma_i^K \int_K b^K dx = (\beta_i^K - \frac{1}{3})|K|,$$

again because u^h and the flux is linear in K.

Now,

$$\omega_i = \varphi_i + \left\{ \begin{array}{ll} \sum_{K, i \in K} \gamma_i^K b^K & \text{if } x \in \text{support of } \varphi \\ 0 & \text{else} \end{array} \right. \tag{34}$$

is *a continuous function*, so that it can be used in the variational formulation.

Denoting by $W_h = \text{span}(\omega_i)$ and $V_h = \text{span}(\varphi_i)$, the problem is: find $u^h \in V^h$ such that for all $w \in W_h$,

$$\int_\Omega w(\nabla f(u^h) - \varepsilon \Delta u^h) dx = 0$$

(I omit the BCs for short and do some abuse of language). If one specifies for ω_i, we get

$$\sum_{K \ni i} \int_K \omega_i \nabla f(u^h) + \varepsilon \int_K \nabla \omega_i \nabla u^h dx = 0$$

The first term gives back $\beta_i^K \phi^K$. Let us have a look at the second one,

$$\int_K \nabla \omega_i \nabla u^h dx = \int_K \nabla \varphi_i \nabla u^h dx + \gamma_i^K \int_K \nabla b^K \nabla u^h dx.$$

since ∇u^h is constant, we see that

$$\int_K \nabla b^K \nabla u^h dx = \nabla u^h \times \int \nabla b^K dx,$$

and by Green formula,

$$\int \nabla b^K = \int_{\partial K} b^K \vec{n} = 0$$

This shows that the variational formulation is

$$\sum_{K\ni i} \beta_i^K \phi^K + \varepsilon \int_K \nabla\varphi_i \nabla u dx = 0$$

i.e. RDS on the convection *plus* Galerkin on the diffusion.

How can we, can we, extend this to higher order, since the key argument here was that the gradient or the divergence of a linear filed is constant. We note in passing that the argument depends also on the fact that the elements are triangles.

Extension to higher degrees. We want to find functions $\gamma_\sigma^K \in H^1(K)$ such that for any degree of freedom $\sigma \in K$:

1. when we use a $\mathbb{P}^k$ Lagrange interpolant,

$$\int_K (\varphi_\sigma + \gamma_\sigma^K)\nabla\cdot f(u^h)dx = \beta_\sigma^K \int_K \nabla\cdot f(u^h)dx, \tag{35a}$$

2.
$$(\gamma_\sigma^K)_{|\partial K} = 0, \tag{35b}$$

3.
$$\int_K \gamma_\sigma^K \Delta u dx = \int_K \text{ div } (\gamma_\sigma^K \nabla u) - \int_K \nabla\gamma_\sigma^K \cdot \nabla u dx = 0$$

that is (because $(\gamma_\sigma^K)_{|\partial K} = 0$,

$$\int_K \nabla\gamma_\sigma^K \cdot \nabla u dx = 0 \tag{35c}$$

for any $u \in \mathbb{P}^k(K)$

We can rephrase (35a) as

$$\int_K \gamma_\sigma^K \nabla\cdot f(u^h)dx = \beta_\sigma^K \int_K \nabla\cdot f(u^h)dx - \int_K \varphi_\sigma \nabla\cdot f(u^h). \tag{36}$$

There is, in general, no solution to this problem. Consider the simple 1D case, with quadratic elements. Consider an element $[x_i, x_{i+1}]$ and by a linear mapping, we can assume that $[x_i, x_{i+1/2}] = [0, 1]$. The Lagrange points σ are 0, 1/2 and 1 and the Lagrange functions are

$$\varphi_0(x) = (1-2x)(1-x), \quad \varphi_0'(x) = 4x-3$$

$$\varphi_{1/2}(x) = 4x(1-x), \qquad \varphi_{1/2}'(x) = 4-8x$$

$$\varphi_1(x) = x(2x-1), \qquad \varphi_1'(x) = 4x-1$$

Since the second derivative of quadratic functions are constant, (35c) writes

$$\int_0^1 \gamma_\sigma dx = 0$$

so that (36) becomes

$$4\int_0^1 \gamma_\sigma x dx = -\beta_\sigma - \int_0^1 \varphi_\sigma \varphi_0'(x) dx$$

$$-8\int_0^1 \gamma_\sigma x dx = -\int_0^1 \varphi_\sigma \varphi_{1/2}'(x) dx$$

$$4\int_0^1 \gamma_\sigma x dx = \beta_\sigma - \int_0^1 \varphi_\sigma \varphi_1'(x) dx$$

If one takes $\sigma = 1/2$, we see that

$$\int_0^1 \gamma_\sigma x dx = 0$$

so that $\beta_{1/2}$ is a given constant.

Let us show that in general, $\beta_{1/2}$ can be arbitrary in $[0,1]$. To show that, we consider the limited scheme constructed from the Lax Friedrichs scheme,

$$\phi_\sigma = \frac{1}{3}(u_1 - u_0) + \alpha(u_\sigma - \bar{u}).$$

We introduce

$$p = \frac{u_{1/2} - u_0}{u_1 - u_0} \text{ and } q = \frac{u_1 - u_{1/2}}{u_1 - u_0}$$

We have $p + q = 1$ and the ratios

$$x_0 = \frac{\phi_0}{\phi} = \frac{1}{3} - \alpha\frac{p+1}{3}$$

$$x_{1/2} = \frac{\phi_{1/2}}{\phi} = \frac{1}{3} + \alpha\frac{p-q}{3}$$

$$x_1 = \frac{\phi_{1/2}}{\phi} = \frac{1}{3} + \alpha\frac{q+1}{3}.$$

If $\alpha = 1$, we have some simplifications

$$x_0 = -\frac{p}{3}, \quad x_{1/2} = 2\frac{p}{3}, \quad x_1 = \frac{3-p}{3}.$$

We see that if $p \in [0,3]$, we have

$$\beta_0 = 0, \quad \beta_{1/2} = \frac{2p}{3+p}, \quad \beta_1 = \frac{3-p}{3+p}$$

and the image of $[0,3]$ by $p \mapsto \dfrac{2p}{3+p}$ is $[0,1]$: $\beta_{1/2}$ can be arbitrary in $[0,1]$. This clearly shows that there is no solution to the problem in general, and that something else must be done.

This version is precisely the one that has been used in section 6.2.1 and the present analysis shows its limits.

7 Conclusion and perspectives.

We have presented the basic elements that enable to construct non oscillatory residual distribution schemes on hybrid meshes, for steady and unsteady problems. These schemes have been tested in 2 and 3 space dimensions with excellent results. These schemes have also been extended to different physical problems, such as the Shallow Water equations and the ideal MHD ones. We refer to the references indicated in the text for further details. It is also possible to adapt the method to discontinuous elements, see [16, 7, 2] for different versions. The idea, as shown in [7] can be adapted to Discontinuous Galerkin schemes.

There is still a lot to be done. Our main efforts are currently on the approximation of the Navier Stokes equations and the use of non Lagrange element to further increase the robustness of the scheme, for example for very strong shocks, see [8]. Concerning viscous problem, we also mention the work of N. Villedieu and co authors [33] for specific forms of the RD schemes. In that reference, they use a special form of the RD scheme, introduced in [6], where the technique of section 6.2.2 can be used. This leads to an efficient scheme, but unfortunately, it does not "degenerate" to a non oscillatory one when viscosity tends to 0.

The section 6.2.2 ended with a rather pessimistic conclusion, but we are currently working on two promissing methods that seems to overcome the problems.

Acknowledgments.

The author has been supported by the FP7 Advanced Grant # 226316 "ADDECCO". The help of Mario Richiuto (INRIA) and A. Larat (now FRG, Stanford) are warmly acknowledged.

References

[1] R. Abgrall. Toward the ultimate conservative scheme: Following the quest. *J. Comput. Phys.*, 167(2):277–315, 2001.

[2] R. Abgrall. A residual distribution method using discontinuous elements for the computation of possibly non smooth flows. *Adv. Appl. Math. Mech.*, 2(1):32–44, 2010.

[3] R. Abgrall, N. Andrianov, and M. Mezine. Towards very high-order accurate schemes for unsteady convection problems on unstructured meshes. *Int. J. Numer. Methods Fluids*, 47(8-9):679–691, 2005.

[4] R. Abgrall, R. Huart, and M. Ricchiuto. Approximation of the ideal mhd equations using residual distribution methods. *in preparation*, 2010.

[5] R. Abgrall, A. Larat, M. Ricchiuto, and C. Tavé. A simple construction of very high order non-oscillatory compact schemes on unstructured meshes. *Computers and Fluids*, 38(7):1314–1323, 2009.

[6] R. Abgrall and P. L. Roe. High-order fluctuation schemes on triangular meshes. *J. Sci. Comput.*, 19(1-3):3–36, 2003.

[7] R. Abgrall and C.W. Shu. Development of residual distribution schemes for the discontinuous galerkin method: The scalar case with linear elements. *Communication in Computational Physics*, 5:376–390, 2009.

[8] R. Abgrall and J. Treflick. An example of high order residual distribution scheme using non lagrange elements. *Journal of Scientific Computing*, 2010. in press.

[9] Rémi Abgrall. Residual distribution schemes: current status and future trends. *Comput. Fluids*, 35(7):641–669, 2006.

[10] Rémi Abgrall and Mohamed Mezine. Construction of second order accurate monotone and stable residual distribution schemes for unsteady flow problems. *J. Comput. Phys.*, 188(1):16–55, 2003.

[11] Bernardo Cockburn and Chi-Wang Shu. The local discontinuous Galerkin method for time-dependent convection-diffusion systems. *SIAM J. Numer. Anal.*, 35(6):2440–2463, 1998.

[12] H. Deconinck, P.L. Roe, and R. Struijs. A multidimensional generalisation of Roe's difference splitter for the Euler equations. *Computer and Fluids*, 22(2/3):215–222, 1993.

[13] H. Deconinck, R. Struijs, G. Bourgeois, and P.L. Roe. Compact advection schemes on unstructured meshes. VKI Lecture Series 1993–04, Computational Fluid Dynamics, 1993.

[14] H. Deconinck, R. Struijs, G. Bourgeois, and P.L. Roe. Compact advection schemes on unstructured meshes. VKI Lecture Series 1993–04, Computational Fluid Dynamics, 1993.

[15] M Hubabrd and M Ricchiuto. Discontinuous upwind residual distribution: A route to unconditional positivity and high order accuracy. *Computers and Fluids*, submitted, 2010.

[16] Matthew Hubbard. Discontinuous fluctuation distribution. *J. Comput. Phys.*, 227(24):10125–10147, 2008.

[17] Th.J.R. Hughes, L.P. Franca, and M. Mallet. Finite element formulation for Computational Fluid Dynamics : I symmetric forms of the compressible Euler and Navier Stokes equations and the secoond law of thermodynamics. *Computer Methods in Applied Mechanics and Engineering*, 54:223–234, 1986.

[18] Th.J.R. Hughes, M. Mallet, and A. Mizukami. A new finite element formulation for Computational Fluid Dynamics : II Beyong SUPG. *Computer Methods in Applied Mechanics and Engineering*, 54:341–355, 1986.

[19] Thomas J.R. Hughes and Michel Mallet. A new finite element formulation for computational fluid dynamics. IV: A discontinuity-capturing operator for multidimensional advective-diffusive systems. *Comput. Methods Appl. Mech. Eng.*, 58:329–336, 1986.

[20] Claes Johnson, Uno Nävert, and Juhani Pitkäranta. Finite element methods for linear hyperbolic problems. *Comput. Methods Appl. Mech. Eng.*, 45:285–312, 1984.

[21] A Larat. *Conception et Analyse de Schémas Distribuant le Résidu d'Ordre Trés Élevé. Application à la Mécanique des Fluides.* PhD thesis, Université de Bordeaux, 2009. http://tel.archives-ouvertes.fr/tel-00502429/fr/.

[22] R.-H. Ni. A multiple grid scheme for solving the Euler equations. *AIAA J.*, 20:1565–1571, 1981.

[23] H. Paillère. *Multidimensional Upwind residual Discretisation Schemes for the Euler and Navier Stokes Equations on Unstructured Meshes.* PhD thesis, Université Libre de Bruxelles, 1995.

[24] M Ricchiuto and R. Abgrall. Explicit runge-kutta residual distribution schemes for time dependent problems: Second order case. *J. Comput. Phys.*, 229(16):5653–5691, 1ugust 2010.

[25] M. Ricchiuto, N. Villedieu, R. Abgrall, and H. Deconinck. On uniformly high-order accurate residual distribution schemes for advection-diffusion. *J. Comput. Appl. Math.*, 215(2):547–556, 2008.

[26] Mario Ricchiuto and Andreas Bollermann. Stabilized residual distribution for shallow water simulations. *J. Comput. Phys.*, 228(4):1071–1115, 2009.

[27] Mario Ricchiuto, Árpád Csík, and Herman Deconinck. Residual distribution for general time-dependent conservation laws. *J. Comput. Phys.*, 209(1):249–289, 2005.

[28] P. L. Roe. Characteristic-based schemes for the euler equations. *Annu. Rev. Fluid Mech.*, 18:337–365, 1986.

[29] P.L. Roe. Approximate riemann solver, parameter vectors and difference schemes. *J. Comput. Phys.*, 43:357–372, 1981.

[30] R. Struijs, H. Deconinck, and P. L. Roe. Fluctuation Splitting Schemes for the 2D Euler equations. *VKI LS 1991-01, Computational Fluid Dynamics*, 1991.

[31] R. Struijs, H. Deconinck, and P.L. Roe. Fluctuation splitting schemes for the 2D Euler equations. VKI LS 1991-01, 1991. Computational Fluid Dynamics.

[32] Bram van Leer. Towards the ultimate conservative difference scheme. IV: A new approach to numerical convection. *J. comput. Phys.*, 23:276–299, 1977.

[33] N. Villedieu, T. Quintino, M. Ricchiuto, and H. Deconinck. A third order residual distribution scheme for the navier stokes equations. *J. Comput. Phys.*, 2010.

[34] Paul Woodward and Phillip Colella. The numerical simulation of two-dimensional fluid flow with strong shocks. *J. Comput. Phys.*, 54:115–173, 1984.

Centre de recherche INRIA Bordeaux – Sud Ouest
Domaine Universitaire - 351, cours de la Libération - 33405 Talence Cedex (France)

Centre de recherche INRIA Grenoble – Rhône-Alpes : 655, avenue de l'Europe - 38334 Montbonnot Saint-Ismier
Centre de recherche INRIA Lille – Nord Europe : Parc Scientifique de la Haute Borne - 40, avenue Halley - 59650 Villeneuve d'Ascq
Centre de recherche INRIA Nancy – Grand Est : LORIA, Technopôle de Nancy-Brabois - Campus scientifique
615, rue du Jardin Botanique - BP 101 - 54602 Villers-lès-Nancy Cedex
Centre de recherche INRIA Paris – Rocquencourt : Domaine de Voluceau - Rocquencourt - BP 105 - 78153 Le Chesnay Cedex
Centre de recherche INRIA Rennes – Bretagne Atlantique : IRISA, Campus universitaire de Beaulieu - 35042 Rennes Cedex
Centre de recherche INRIA Saclay – Île-de-France : Parc Orsay Université - ZAC des Vignes : 4, rue Jacques Monod - 91893 Orsay Cedex
Centre de recherche INRIA Sophia Antipolis – Méditerranée : 2004, route des Lucioles - BP 93 - 06902 Sophia Antipolis Cedex

Éditeur
INRIA - Domaine de Voluceau - Rocquencourt, BP 105 - 78153 Le Chesnay Cedex (France)
http://www.inria.fr
ISSN 0249-6399